Vertical structure, energetics, and dynamics of the Brazil Current System at 22°S–28°S

Cesar B. Rocha,[1,2] Ilson C. A. da Silveira,[1] Belmiro M. Castro,[1] and Jose Antonio M. Lima[3]

Received 24 May 2013; revised 28 November 2013; accepted 2 December 2013; published 7 January 2014.

[1] We use four current meter moorings and quasi-synoptic hydrographic observations in conjunction with a one-dimensional quasi-geostrophic linear stability model to investigate downstream changes in the Brazil Current (BC) System between 22°S and 28°S. The data set depict the downstream thickening of the BC. Its vertical extension increases from 350 m at 22.7°S to 850 m at 27.9°S. Most of this deepening occurs between 25.5°S and 27.9°S and is linked to the bifurcation of the South Equatorial Current at intermediate depths (Santos bifurcation), which adds the Antarctic Intermediate Water flow to the BC. Geostrophic estimates suggest that the BC transport is increased by at least 4.3 Sv (∼70%) to the south of that bifurcation. Moreover, the Santos bifurcation is associated with a substantial increase in the barotropic component of the BC System. On average, the water column average kinetic energy (IKE) is 70% baroclinic to the north and 54% barotropic to the south of the bifurcation. Additionally, the BC shows conspicuous mesoscale activity off southeast Brazil. The water column average eddy kinetic energy accounts for 30–60% of the IKE. Instabilities of the mean flow may give rise to these mesoscale fluctuations. Indeed, the linear stability analysis suggests that the BC System is baroclinically unstable between 22°S and 28°S. In particular, the model predicts southwestward-propagating fastest growing waves (∼190 km) from 25.5°S to 27.9°S and quasi-standing most unstable modes (∼230 km) at 22.7°S. These modes have vertical structures roughly consistent with the observed eddy field.

Citation: Rocha, C. B., I. C. A. da Silveira, B. M. Castro, and J. A. M. Lima (2014), Vertical structure, energetics, and dynamics of the Brazil Current System at 22°S–28°S, *J. Geophys. Res. Oceans*, *119*, 52–69, doi:10.1002/2013JC009143.

1. Introduction

[2] The Brazil Current (BC) is the subtropical western boundary current (WBC) of the South Atlantic. Most of our current understanding of the BC relies on quasi-synoptic hydrographic observations [e.g., *Campos et al*., 1995; *da Silveira et al*., 2004]. Studies based on analysis of current meter time series are rare [*Müller et al*., 1998; *da Silveira et al*., 2008], and this has constrained the development of a quantitative description of the BC.

[3] As it flows over the southeast Brazil slope (∼20°S–25°S), the BC presents a vertical structure very different from that of other WBCs at similar latitudes [*da Silveira et al*., 2008]. In this region, the BC is depicted as a shallow current (∼400 m), transporting tropical water (TW) at surface/near-surface levels and South Atlantic Central Water (SACW) at pycnocline levels [*Campos et al*., 1995; *da Silveira et al*., 2000]. Underneath the BC (∼(500–1200) m), there is an opposing flow, the intermediate western boundary current (IWBC), transporting mainly Antarctic Intermediate Water (AAIW) to the north/northeast [e.g., *Evans and Signorini*, 1985; *da Silveira et al*., 2004]. This unique subtropical WBC System is linked to the depth-dependent bifurcation system of the South Equatorial Current over the Brazilian continental margin [e.g., *Stramma and England*, 1999]. At intermediate levels, float observations suggest that the so-called Santos bifurcation occurs between 25°S and 27°S [*Böebel et al*., 1999; *Legeais et al*., 2013]. To the south of that bifurcation (∼28°S), the entire water column over the slope flows to the south/southwest [*Müller et al*., 1998], and the BC transports TW, SACW, and AAIW.

[4] Few studies have addressed the BC dynamics. *da Silveira et al*. [2008] showed that the mean BC System at 22.7°S is essentially a first baroclinic mode flow. Furthermore, these authors argued that the vertical shear associated with the BC/IWBC opposing flows likely makes the BC System prone to baroclinic instability, and that a one-dimensional quasi-geostrophic (QG) model successfully predicted the length scales of the mesoscale variability in this region. Additionally, the QG linear model predicted unstable modes with very small propagation speeds,

[1]Instituto Oceanográfico, Universidade de São Paulo, São Paulo, Brazil.
[2]Now at Scripps Institution of Oceanography, University of California, San Diego, La Jolla, California, USA.
[3]Centro de Pesquisas e Desenvolvimento Leopoldo A. Miguez de Mello, Petróleo Brasileiro S. A., Rio de Janeiro, Brazil.

Corresponding author: C. B. Rocha, Scripps Institution of Oceanography, University of California, San Diego, 9500 Gilman Drive, La Jolla, CA 92093-0208, USA. (crocha@ucsd.edu)

2169-9275/14/10.1002/2013JC009143

Table 1. Main Characteristics for the MARLIM, DFBS, C3, and W333 Moorings[a]

	Isobath (m)	Instruments (m)	Record (Days)	Reference
MARLIM (22.7°S, 40.2°W)	1250	50; 100; 250; 350; 450; 650; 750; 950; 1050	308 (Feb 1992 to Dec 1992)	*da Silveira et al*. [2008]
DFBS (24.15°S, 42.4°W)	1200	30; 50; 70; 500;800; 1000	482 (Jan 2003 to May 2004)	—
C3 (25.5°S, 44.9°W)	1000	29; 91; 293; 698	455 (Dec 1992 to Mar 1994)	*Campos et al*. [1996]
W333 (27.9°S, 46.7°W)	1200	60; 77; 95; 112; 138; 155; 173; 230; 475; 680; 885	693 (Jan 1991 to Nov 1992)	*Müller et al*. [1998]

[a]Note that *da Silveira et al*. [2008] only used the second half of the MARLIM record and *Campos et al*. [1996] only quoted the C3 mooring results.

roughly in agreement with the few observed events in sea surface temperature imagery [*Garfield*, 1990]. *Mano et al*. [2009] described the energy flux during the growth of a cyclonic meander in a primitive-equation (PE) numerical simulation of the BC System in the same region. While the basic phenomenology described by these authors is qualitatively consistent with *da Silveira et al*.'s [2008] QG baroclinic instability arguments, the BC meandering seems to be much more complicated in the PE model. Additionally, *Oliveira et al*. [2009] studied the surface energetics of the BC from surface drifter buoys. These authors showed that the (surface) eddy kinetic energy is significant along the BC path. Based on barotropic conversion estimates, *Oliveira et al*. [2009] argued that part of the BC variability may be accounted for by barotropic instabilities.

[5] It is relatively well accepted that the BC undergoes changes on its downstream path off southeast Brazil [*Müller et al*., 1998; *da Silveira et al*., 2000]. Nonetheless, no systematic quantifications of these changes are available to date. In addition, the BC is generally associated with rich mesoscale activity within this region [e.g., *Campos et al*., 1995, 2000; *da Silveira et al*., 2008], but quantitative estimates of its importance are limited to the surface [*Oliveira et al*., 2009].

[6] Here, we investigate downstream changes in the BC between 22°S and 28°S. The specific questions are: (1a) How much does the BC thicken and (1b) how much does the BC transport increase within this region? (2a) What is the partition between barotropic and baroclinic components in the BC System and (2b) what are the downstream changes on this partition? (3) How much of the BC System energy is in the eddy field? (4a) What are the downstream changes in the BC System linear stability properties and (4b) can the predictions of the stability analysis account for the changing character of the perturbations in the downstream direction?

[7] To address these questions, we analyze four current meter mooring records, not necessarily spanning the same time period, but nonetheless covering the study region with unprecedented along-coast resolution. The analysis of these moorings within the same framework combined with quasi-synoptic hydrographic observations yields a comprehensive (but limited) description of the BC off southeast Brazil. In addition, application of a QG model to the observations provides insight into the dynamics governing the BC variability at mesoscales.

2. Mooring Observations

2.1. The Data Set

[8] The four current meter moorings were located in the BC domain (Figure 5 and Table 1) spanning the southeast Brazil (22°S–28°S): MARLIM (22.7°S, 1250 m), DEPROAS FBS (24.15°, 1200 m; hereafter DFBS), COROAS 3 (25.5°, 1000 m; hereafter C3), and WOCE ACM12 333 (27.9°S, 1200 m; hereafter W333). These records span 1–2 years; thus the BC mesoscale variability is expected to be well resolved.

[9] The velocity record at each current meter was low-pass filtered using a Lanczos-cosine filter [e.g., *Emery and Thomson*, 2001]. The cutoff period was set at 40 h, which is 30% greater than the inertial period at the northernmost mooring (~31 h), and therefore near-inertial and superinertial motions were filtered out. Individual current meter gaps were filled using the empirical orthogonal functions (EOF) of the velocity anomaly time series. This technique was chosen because it does not change the data statistics [*Beckers and Rixen*, 2003; *Dengler et al*., 2004; *Schott et al*., 2005].

[10] The C3 mooring had a gap in all four instruments (4 May 1993 to 18 June 1993), which was filled in two steps. The uppermost instrument velocity series was filled using the EOF method (horizontally) with the uppermost instrument of an adjacent mooring which had a spectrum coherent with the C3 mooring uppermost record. The remaining gaps in the other three instruments were then filled using the EOFs (vertically). Such a twofold filling process was not possible for the 30 day gap (27 May 1992 to 23 June 1992) at the MARLIM mooring since concurrent adjacent moorings were not available.

[11] The BC flow is clearly depicted in the upper 300 m at the MARLIM mooring (Figure 1), although strong current reversals are also observed in the upper levels. As near-inertial and superinertial motions were filtered out, it is likely that these reversals are due to strong BC meandering events [*da Silveira et al*., 2008]. The IWBC is consistently depicted from 650 to 1050 m flowing to the northeast. No current reversals are observed in the IWBC domain, suggesting that the meandering is mainly confined to the upper levels.

[12] The time series for the DFBS mooring depicts a much more convoluted scenario (Figure 2). The three uppermost instruments present strong current reversals throughout the record. At intermediate levels (800 and 1000 m instruments) this mooring depicts the IWBC flowing to the northeast. However, it should be noted that the IWBC seems more variable at this location than at the MARLIM mooring. The flow at 500 m presents reversals throughout the record, suggesting that the separation of the BC-IWBC occurs near this depth.

[13] At the C3 mooring (Figure 3), the BC is depicted in the three upper instruments as a persistent southwest flow.

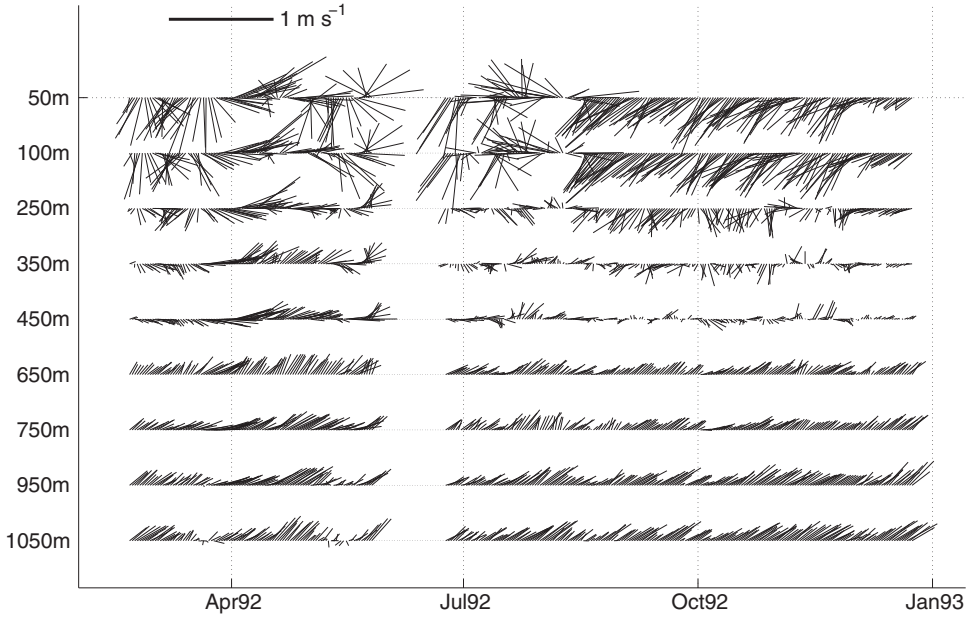

Figure 1. MARLIM mooring velocity time series. Only one vector per day is plotted. For reference, the north points upward.

Although the BC is also highly variable at this location, just one strong current reversal was observed (March 1993). The C3 mooring has just one instrument at intermediate depths (693 m), which depicts a northeastward flow. This suggests that the IWBC is already well formed at this location, as suggested by *Campos et al*. [1996]. However, it is important to note that, contrary to what is observed at the MARLIM mooring, the northeast flow at the C3 mooring is clearly highly variable.

[14] Farther downstream at the W333 mooring (Figure 4), the BC is depicted flowing southward/southwestward from the surface down to the instrument at 670 m depth. At this location, just two prominent velocity vector reversals are depicted in the BC (January 1991 and October 1992). In addition, the flow at the deepest instrument (885 m) is highly variable and presents no preferential direction. Thus, there is no evidence of the IWBC, suggesting that this mooring is located to the south of the Santos bifurcation. This is consistent with a recent description on the basis of float observations [*Legeais et al*., 2013].

2.2. Basic Velocity Statistics

[15] A well-known caveat in mooring data analysis is that instruments, particularly those near the surface, may experience substantial drawn down during highly energetic events. This can bias statistical analyses, but there seems to be no easy solution for such problem [*Wunsch*, 1997]. For the present data set, we have reliable pressure records only for the W333 mooring. At this location, the vertical displacements are typically fairly small (<30 m about the nominal depth), but can be as large as 175 m in one extreme short-lived case. The 230 m instrument was 90% of the time at depths shallower than 255 m, which represents a displacement of 10% about its nominal depth. Assuming that the other three moorings experienced similar small vertical displacements, the statistics presented below are deemed reliable.

[16] It is convenient to rotate the velocity vector into a local along-front/cross-front coordinate system since this

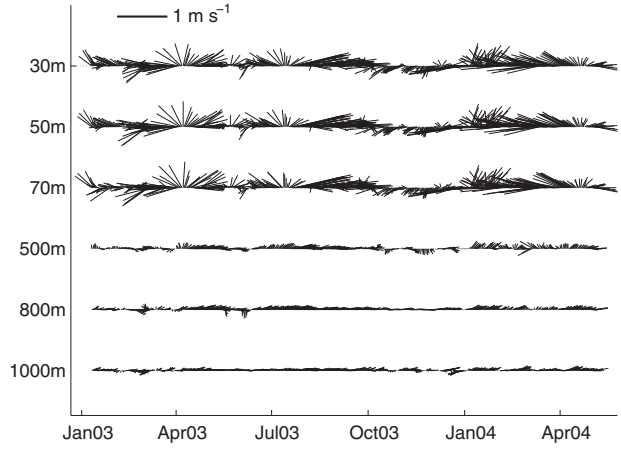

Figure 2. Similar to Figure 1, but for the DFBS mooring.

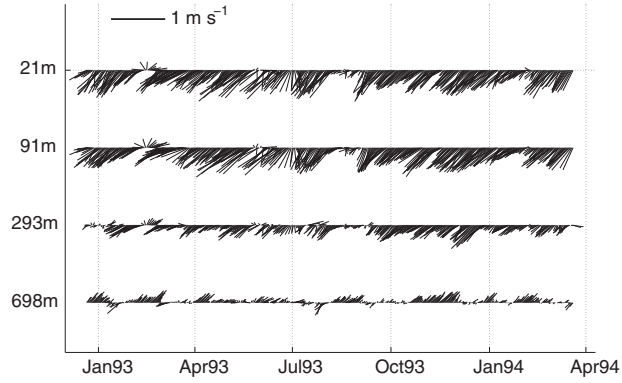

Figure 3. Similar to Figure 1, but for the C3 mooring.

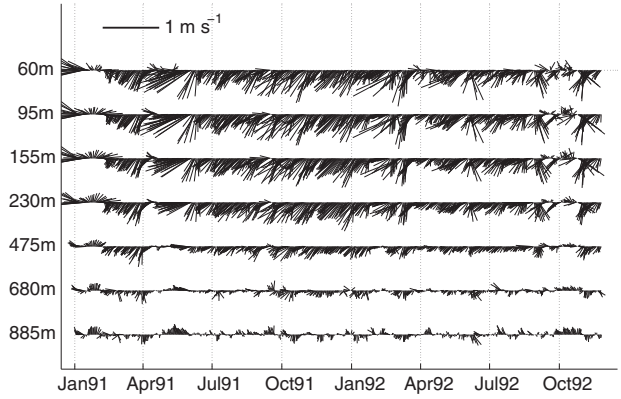

Figure 4. Similar to Figure 1, but for the W333 mooring. The velocity records at 77, 112, 138, and 173 m are omitted.

facilitates the intercomparison among the moorings. The BC thermal front marks the BC inshore border [*Garfield*, 1990; *da Silveira et al*., 2008]. The along-front direction was computed based on the angle between geographic north and the BC mean thermal front, which was computed using the estimates of *Garfield* [1990] and *da Silveira et al*. [2008] (Figure 5); at the DFBS mooring, where those estimates diverge, we used the mean thermal front from the latter authors. Hereafter, *u* and *v* will be used to refer to the local cross-front and along-front (low-pass filtered) velocity components, respectively.

[17] For each mooring, basic statistics (mean and standard deviation) for the velocity components were estimated. In order to assess the robustness of these estimates, standard errors were calculated [e.g., *Glover et al*., 2011]. The standard error depends on the standard deviation as well as on the effective number of degrees of freedom (eDOF). The eDOF was computed by dividing the record length by the (autocorrelation) integral time scale [*Glover et al*., 2011]. Integral time scale and eDOF were computed individually for each velocity component at each current meter.

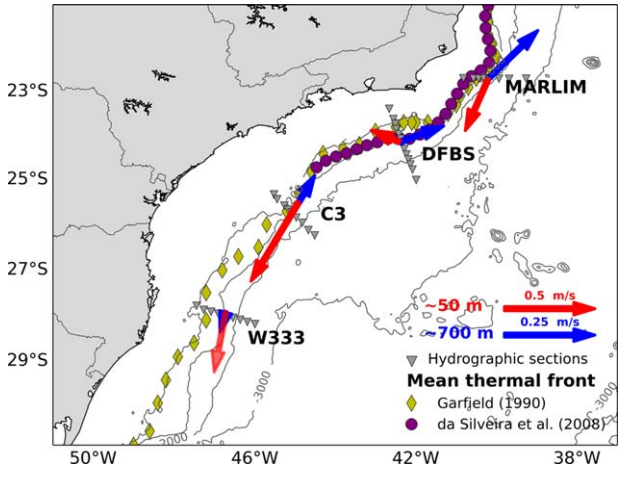

Figure 5. Mean velocity vector for instruments closest to 50 m (red) and 700 m (blue) at each mooring. The mean thermal front estimated by *Garfield* [1990] (diamonds) and *da Silveira et al*. [2008] (circles) are also shown. Gray triangles represent hydrographic stations.

Table 2. Velocity Statistics for the MARLIM Mooring[a]

Instrument (m)	Along Front		Cross Front	
	Mean (m s^{-1})	Std (m s^{-1})	Mean (m s^{-1})	Std (m s^{-1})
50	-0.31 ± 0.12	0.37 ± 0.08	$0.07 \pm 0.08^{*}$	0.25 ± 0.06
100	-0.26 ± 0.11	0.36 ± 0.08	0.08 ± 0.07	0.23 ± 0.05
250	-0.08 ± 0.06	0.20 ± 0.04	0.08 ± 0.04	0.13 ± 0.03
350	$0.02 \pm 0.05^{*}$	0.16 ± 0.03	0.05 ± 0.03	0.09 ± 0.02
450	0.08 ± 0.03	0.10 ± 0.02	0.07 ± 0.03	0.09 ± 0.02
650	0.19 ± 0.02	0.07 ± 0.02	$0.00 \pm 0.01^{*}$	0.05 ± 0.01
750	0.19 ± 0.02	0.07 ± 0.01	0.03 ± 0.02	0.06 ± 0.01
950	0.22 ± 0.03	0.08 ± 0.02	0.03 ± 0.01	0.04 ± 0.01
1050	0.21 ± 0.03	0.10 ± 0.02	0.02 ± 0.01	0.03 ± 0.01

[a]The 95% confidence interval was computed by doubling the standard error. Stars indicate those estimates that are not statistically significant.

[18] The time scales proved to be anisotropic, which led to significant differences in the eDOF in each direction. The along-front integral time scale varies from 6 to 9 days, whereas the cross-front integral time scale ranges from 4 to 5 days. Moreover, eDOF varies substantially (∼30–170) from mooring to mooring due to differences in the duration of the records.

[19] Mean and standard deviation along with their uncertainties are presented in Tables (2–5), and the mean velocity vectors for the instruments closest to 50 and 700 m are displayed in Figure 5. The mean flow essentially follows the mean BC thermal front, which is parallel to the local isobath at all moorings except at the DFBS mooring (Figure 5). Near this mooring, the mean BC front veers westward along the 200 m isobath; the veering of the deeper isobaths is gentler, so that the IWBC flow at this location follows the local isobath, which is not in the same direction as the BC front.

[20] The near-surface BC along-front mean velocity is highest at the C3 mooring (-0.51 ± 0.05 m s^{-1} at 29 m), as compared to the W333 mooring (-0.34 ± 0.04 m s^{-1} at 60 m) and MARLIM mooring (-0.31 ± 0.12 m s^{-1} at 50 m). This suggests that the C3 mooring is closer to the BC core than the other moorings. Furthermore, at the DFBS mooring, the mean along-front BC velocity is much weaker (-0.17 ± 0.14 m s^{-1} at 50 m). Near-surface along-front standard deviation is higher at the DFBS mooring (0.39 ± 0.10 m s^{-1} at 50 m) and at the MARLIM mooring (0.37 ± 0.03 m s^{-1} at 50 m), exceeding the mean values at their respective depths, thus confirming the high variability

Table 3. Similar to Table 2, but for the DFBS Mooring

Instrument (m)	Along Front		Cross Front	
	Mean (m s^{-1})	Std (m s^{-1})	Mean (m s^{-1})	Std (m s^{-1})
30	-0.17 ± 0.14	0.38 ± 0.10	$0.02 \pm 0.04^{*}$	0.17 ± 0.03
50	-0.17 ± 0.14	0.39 ± 0.10	$0.02 \pm 0.04^{*}$	0.18 ± 0.03
70	-0.16 ± 0.14	0.40 ± 0.10	$0.02 \pm 0.04^{*}$	0.19 ± 0.03
500	$0.04 \pm 0.04^{*}$	0.12 ± 0.03	0.04 ± 0.01	0.06 ± 0.01
800	0.11 ± 0.03	0.08 ± 0.02	0.07 ± 0.01	0.04 ± 0.01
1000	0.09 ± 0.03	0.09 ± 0.02	0.05 ± 0.01	0.04 ± 0.01

Table 4. Similar to Table 2, but the for C3 Mooring

Instrument (m)	Along Front		Cross Front	
	Mean (m s^{-1})	Std (m s^{-1})	Mean (m s^{-1})	Std (m s^{-1})
29	-0.51 ± 0.05	0.24 ± 0.04	$-0.01 \pm 0.03^{*}$	0.12 ± 0.02
91	-0.49 ± 0.06	0.24 ± 0.04	-0.05 ± 0.03	0.12 ± 0.02
293	-0.23 ± 0.04	0.17 ± 0.03	-0.03 ± 0.01	0.06 ± 0.01
698	0.09 ± 0.03	0.13 ± 0.02	$0.00 \pm 0.01^{*}$	0.03 ± 0.01

at these locations. Relatively high near-surface along-front standard deviation values are also observed at the C3 mooring (0.24 ± 0.04 m s^{-1} at 29 m) and at the W333 mooring (0.23 ± 0.03 m s^{-1} at 60 m). The high uncertainties associated with the mean estimates at near-surface instruments at the DFBS and MARLIM moorings are a consequence of the small eDOF and the high standard deviation at those locations. In particular, the mean values for the three upper instruments at the DFBS mooring have low statistical significance. There are too few eDOF to estimate a reliable along-front mean. Physically, the BC experiences high variability in this region, as if continuously adjusting to conserve its potential vorticity after overshooting the continental margin past Cape Frio (~23°S) [*Campos et al*., 1995]. Therefore, it is very difficult to establish a "stationary" flow at this location.

[21] The BC cross-front mean velocity component is very weak at all moorings (Tables 2–5). Although slightly smaller than those estimates for the along-front component, the standard deviation for the cross-front component is significant, suggesting that the time-varying flow is less anisotropic than the time-mean flow.

[22] At intermediate depths, the MARLIM and DFBS moorings consistently depict a mean IWBC flowing northeastward. Maximum IWBC along-front velocity is observed in the north of the domain, at the MARLIM mooring (0.22 ± 0.03 m s^{-1} at 950 m). At the DFBS mooring, maximum along-front IWBC velocity is observed at 800 m (0.11 ± 0.02 m s^{-1}). At the C3 mooring, the single instrument at intermediate depths depicts a relatively weak (but significant) northward/eastward flow (0.09 ± 0.03 m s^{-1} at 698 m). The along-front IWBC velocity component seems to present relatively small (relative to the mean) standard deviation values at the MARLIM mooring (0.08 ± 0.02 m s^{-1} at 950 m), but slightly greater at the DFBS mooring (0.08 ± 0.02 m s^{-1} at 800 m). At the C3 mooring, the along-front IWBC standard deviation (0.13 ± 0.02 m s^{-1} at 698 m) exceeds the mean value.

[23] In contrast, a mean southwestward along-front flow is observed at intermediate depths at the W333 mooring (-0.06 ± 0.02 m s^{-1} at 680 m), in agreement with *Müller et al*.'s [1998] estimates. No mean northward/eastward flow is observed at this location. Relatively high along-front standard deviation values are observed at intermediate depths at this mooring, exceeding the mean values (0.10 ± 0.01 m s^{-1} at 680 m).

[24] In summary, the basic statistics shows that the BC presents significant variability off southeast Brazil, thus corroborating the importance of mesoscale activity within this region. The mean along-front velocity measurements also depict the thickening of the BC, namely its downstream growth in vertical extension. In order to better describe this thickening process, we now turn to the projection of the mean along-front velocity profile onto the dynamical modes.

Table 5. Similar to Table 2, but for the W333 Mooring.

Instrument (m)	Along Front		Cross Front	
	Mean (m s^{-1})	Std (m s^{-1})	Mean (m s^{-1})	Std (m s^{-1})
60	-0.34 ± 0.04	0.23 ± 0.03	-0.07 ± 0.03	0.17 ± 0.02
77	-0.34 ± 0.05	0.23 ± 0.03	-0.06 ± 0.04	0.17 ± 0.03
95	-0.34 ± 0.05	0.23 ± 0.03	-0.07 ± 0.04	0.17 ± 0.03
112	-0.34 ± 0.05	0.23 ± 0.03	-0.07 ± 0.03	0.17 ± 0.02
138	-0.33 ± 0.05	0.23 ± 0.03	-0.06 ± 0.03	0.16 ± 0.02
155	-0.32 ± 0.05	0.22 ± 0.03	-0.06 ± 0.03	0.15 ± 0.02
173	-0.31 ± 0.05	0.21 ± 0.03	-0.06 ± 0.03	0.14 ± 0.02
230	-0.29 ± 0.05	0.20 ± 0.03	-0.06 ± 0.03	0.13 ± 0.02
475	-0.15 ± 0.03	0.12 ± 0.02	-0.04 ± 0.01	0.07 ± 0.01
680	-0.06 ± 0.02	0.10 ± 0.01	-0.02 ± 0.01	0.06 ± 0.01
885	$0.00 \pm 0.02^{*}$	0.11 ± 0.01	-0.02 ± 0.01	0.05 ± 0.01

2.3. The Thickening of the Brazil Current

[25] The mean along-front velocity at the discrete instrument depths were fit to the five gravest dynamical modes using a Gauss-Markov estimate [e.g., *Szuts et al*., 2012]. These modes were computed numerically using the mean stratification (N^2 (z)) at each location. N^2 (z) profiles were estimated using the World Ocean Atlas 2009 climatology [*Locarnini et al*., 2010; *Antonov et al*., 2010]. As the dynamical modes and their derivatives are smooth [*da Silveira et al*., 2008], we argue that this is a consistent method for obtaining interpolated velocity profiles on an equispaced grid. These profiles are further used along with the N^2 (z) profile as inputs for the linear stability model (section 5.1).

[26] The interpolated along-front velocity profiles clearly show the thickening of the BC (Figure 6). Accordingly, the BC is 350 m deep at the MARLIM mooring, 550 m deep at the C3 mooring, and 850 m deep at the W333 mooring. Although the mean along-front velocity presents low statistical significance at the DFBS mooring, the BC vertical extension (~400 m) seems to be consistent at this location.

[27] Another interesting feature that is clear in the synthesized velocity profiles concerns the downstream changes in mean flow vertical shear. Accordingly, the BC System presents a much more prominent shear at the MARLIM, DFBS, and C3 moorings than at the W333 mooring, thus suggesting that the Santos bifurcation is associated with a strong increase in the BC System barotropic component.

3. Quasi-Synoptic Patterns

[28] In order to present a two-dimensional characterization of the downstream changes in the BC, we analyze the available hydrographic sections contemporary with the mooring records (Table 6). The W333 does not present velocity measurements exactly concurrent to the A10 cruise. While this cruise recovered the W333 mooring, the last month (December 1992) of the mooring measurements were disregarded during the quality control process. At this location, the mooring velocity compared to the geostrophic velocity estimates represents those measurements made 1

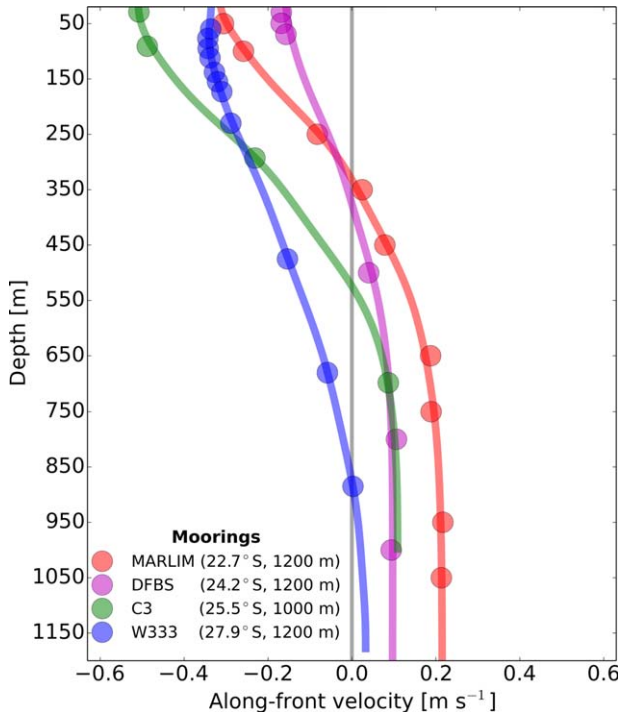

Figure 6. Time mean of the along-front velocity (m s^{-1}) for: MARLIM (22.7°S, red); DFBS (24.15°S, magenta); C3 (25.5°S, green), and W333 (27.9°S, blue). Filled circles indicate the current meter mean values; continuous lines represent a "dynamical fit" to the discrete values.

month earlier (30 November 1992), and hence this comparison should be interpreted with caution.

[29] Geostrophic velocities are computed relative to an isopycnal level of no motion [e.g., *Stramma et al*., 1995]. There is no such reason to expect that the velocity is zero along these isopycnals, although it is likely. This is a source of inaccuracy in the geostrophic velocity estimates, and care should be taken in interpreting the results. Nonetheless, this method proved to produce a consistent (lower bound) transport estimates without requiring arbitrary shoreward extrapolations of the geopotential anomalies to compute velocities on the inner slope. The isopycnal used for reference is the one that crosses the mooring at the corresponding no-motion depth at the mooring location. The mooring data was averaged over the same time period as the section occupation, typically 3 days.

[30] At the MARLIM, DFBS, and C3 moorings, the level of no motion is associated with the depth that separates the BC from the IWBC flow. The reversal depth is estimated from the mooring velocity profile synthesized using the dynamical modes in a fashion similar to the mean flow (section 2.3). At these locations, similar results are obtained by setting an arbitrary level of no motion (not shown). At the W333 mooring the IWCB is not present, and hence there is no such reversal depth. We therefore consider the level of no motion as that of the deepest instrument (885 m), which presented fairly weak velocities during the hydrographic cruise occupation (∼0.03 m s^{-1}). At this mooring, similar results (pattern and transport) are obtained by computing the geostrophic velocities referenced to the bottom (not presented).

[31] The BC geostrophic transport is estimated considering this current as the southward flow delimited by the −0.05 m s^{-1} isotach, which was the weakest contour that defined the BC in all sections. Hence, the transport values presented here represent conservative estimates. The geostrophic velocity estimates are compared to the mooring velocities averaged over the cruise period. For the DFBS, C3, and W333 moorings, which are located between two geostrophic velocity profiles, the mooring velocity is compared against the mean estimate between the two adjacent profiles.

[32] The MARLIM P2 cruise depicts a shallow BC (∼350 m), with maximum (surface) velocity of ∼0.5 m s^{-1} (Figure 7a). The BC is slightly skewed shoreward, although it seems to be flowing essentially over the slope. The northward flow beneath the BC was not entirely sampled because the conductivity-temperature-depth (CTD) casts stopped at 1000 m on this cruise. Nonetheless, the IWBC seems to be a consistent northward flow, with maximum geostrophic velocity of 0.2 m s^{-1} at its core (∼800 m). The BC geostrophic transport is 4.87 Sv, very similar to that obtained by *da Silveira et al*. [2008] on the basis of an application of a sectional version of the Princeton Ocean Model for the same cruise (4.24 Sv). The estimated geostrophic velocity is (at best) satisfactory (Figure 7b). The geostrophic IWBC seems fairly consistent with that measured at the MARLIM mooring. However, the geostrophic velocity overestimates the near-surface moored velocity magnitude and vertical shear. The root-mean-square (RMS) difference between mooring and geostrophic velocity is 0.08 m s^{-1}.

[33] The geostrophic velocity section for the DEPROAS V cruise depicts a relatively shallow BC (∼400 m), with maximum surface velocity of ∼0.8 m s^{-1} (Figure 8a). Underneath the BC, the IWCB is depicted extending to deeps greater than ∼1200 m, with maximum velocity of ∼0.2 m s^{-1} (∼1000 m). During this cruise, a frontal cyclonic meander was observed. The BC geostrophic transport is estimated at 7.02 Sv, greater than a previous estimate close to this location (5.6 Sv) [*da Silveira et al*., 2004]. Moreover, the estimated geostrophic velocity seems fairly consistent with the (cruise average) mooring velocity

Table 6. Hydrographic Cruises Contemporary With Mooring Records

Cruise	Mooring	Occupation Date	Reference Isopycnal[a]	BC Transport
MARLIM P2	MARLIM	17–20 Nov 1992	26.5 kg m^{-3}	4.87 Sv
DEPROAS V	DFBS	27–29 Sep 2003	26.7 kg m^{-3}	7.02 Sv
COROAS HM2	C3	23–25 Jul 1993	26.8 kg m^{-3}	5.73 Sv
WOCE A10	W333	30–31 Dec 1992	27.3 kg m^{-3}	10.02 Sv

[a]Isopycnal level of no motion based on the synthesized mooring velocity (averaged over the cruise period).

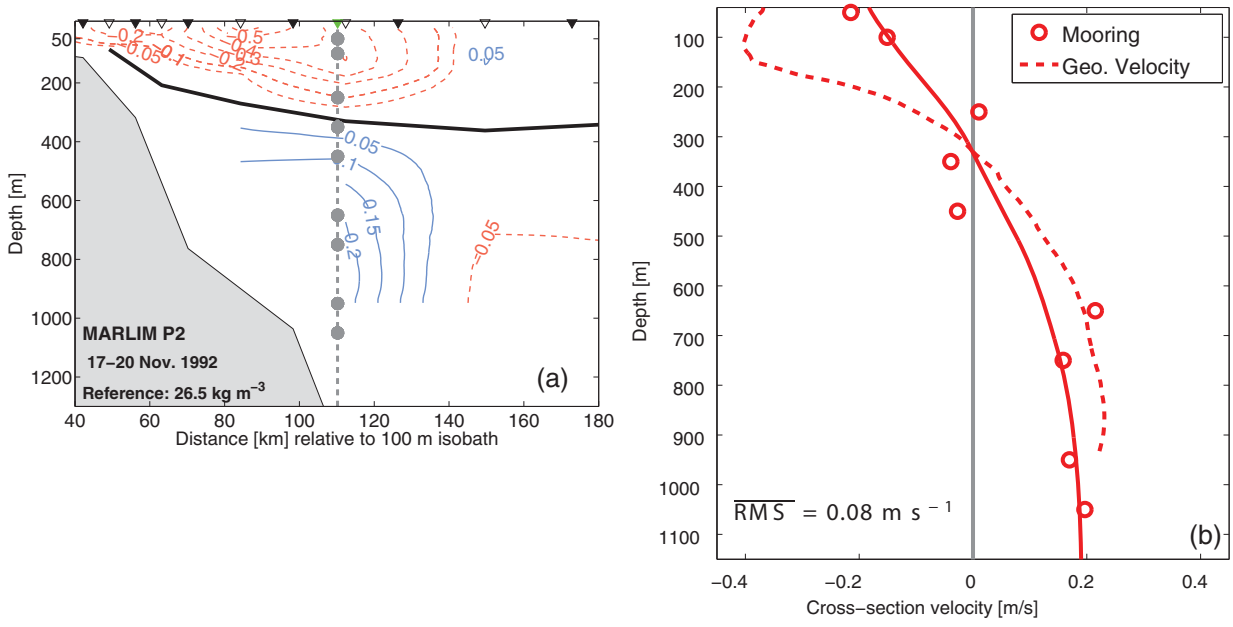

Figure 7. (a) Geostrophic velocity for the MARLIM P2 cruise relative to an isopycnal level of no motion (black line) and (b) comparison of geostrophic velocity and mooring velocity (time mean over the period of the cruise). Black triangles represent the hydrographic stations. White triangles indicate the positions used in the geostrophic velocity calculation. The green triangle represents the point (along the section) closest to the MARLIM mooring. Gray dots indicate the current meter positions along the water column.

(Figure 8b). The RMS difference between the synthesized mooring velocity and the geostrophic velocity is 0.03 m s^{-1}. The major differences consist of an overestimation of the surface velocities and an underestimation of the velocities close to the IWBC core (∼1000 m).

[34] The HM2 cruise depicts a ∼450 m deep BC flowing southward, with maximum (surface) geostrophic velocity of ∼0.8 m s^{-1} (Figure 9a). The IWBC is depicted as a northward flow with maximum velocity of ∼0.15 m s^{-1} at its core (∼1000 m), thus weaker than that during the

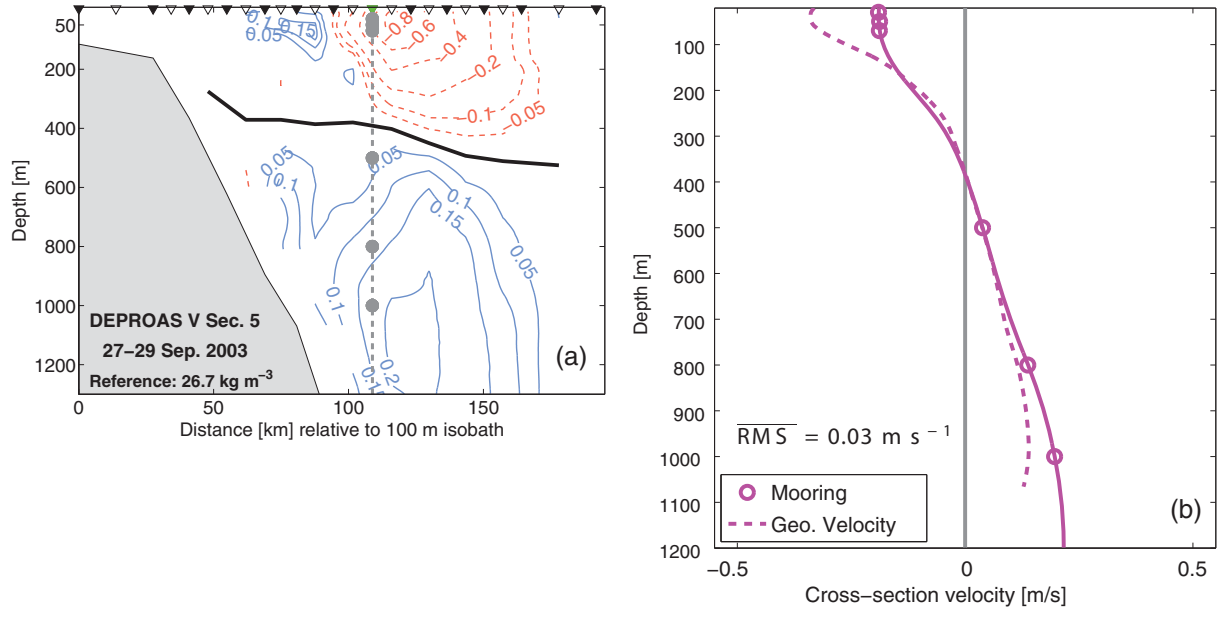

Figure 8. Similar to Figure 7, but for the DEPROAS V cruise/DFBS mooring. As the mooring position is not coincident with a geostrophic velocity profile (white triangles), the latter is taken as the average between the profiles adjacent to the mooring position.

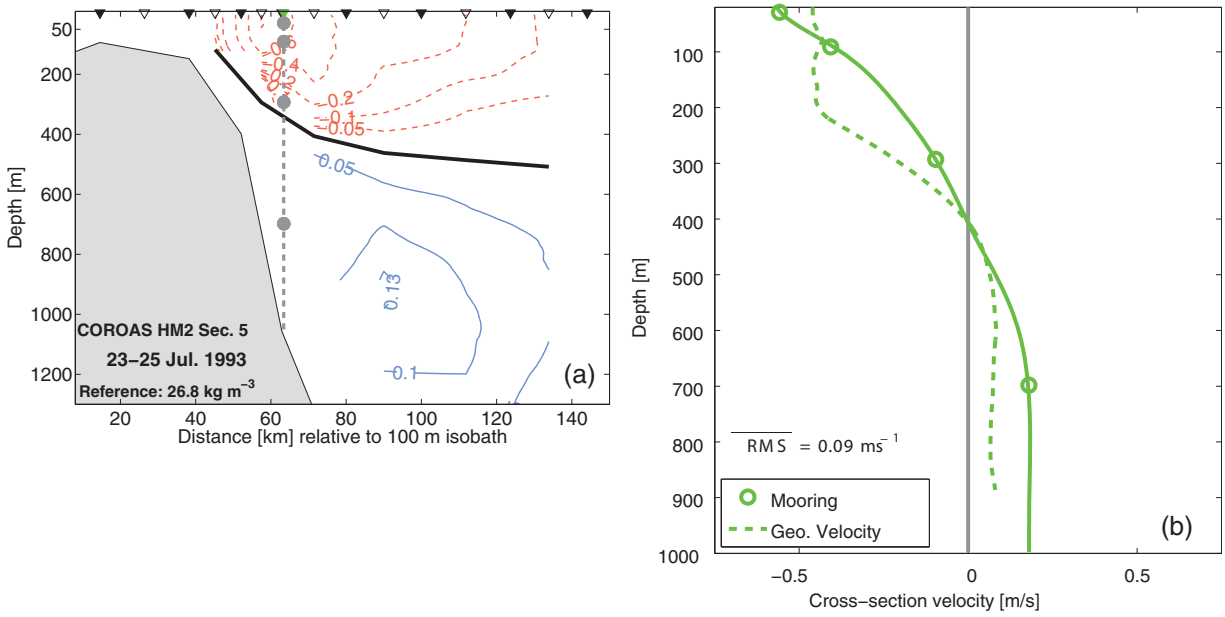

Figure 9. Similar to Figure 7, but for the COROAS HM2 cruise and C3 mooring. As the mooring position is not coincident with a geostrophic velocity profile (white triangles), the latter is taken as the average between the profiles adjacent to the mooring position.

DEPROAS V cruise. At this location, the BC and IWBC cores are not aligned; the IWCB core is displaced offshore. (Considering that this quasi-synoptic depiction is representative of the mean BC, the C3 mooring is located very close to the BC core. This is consistent with the fact that the C3 mooring presented highest velocity as compared to the other moorings.) For this cruise, the BC geostrophic transport is 5.73 Sv, consistent with the estimate by *Campos et al*. [1995], although those authors considered a much deeper level of no motion (5.73 Sv relative to 750 dbar). Nevertheless, we acknowledge that this may be a lower bound estimate since part of the BC seems to be flowing over the outer shelf. The agreement between the geostrophic velocity and that measured by the C3 mooring is satisfactory (Figure 9b). The main difference is an underestimation of the flow close to the IWBC core. The RMS difference between the velocity profiles is 0.09 m s^{-1}.

[35] Farther downstream, the WOCE A10 cruise depicts a significantly different scenario, namely a ∼900 m deep BC, with maximum (surface) velocity of ∼0.55 m s^{-1} (Figure 10a). The BC is also significantly skewed shoreward at this location. Consistent with that observed by the W333

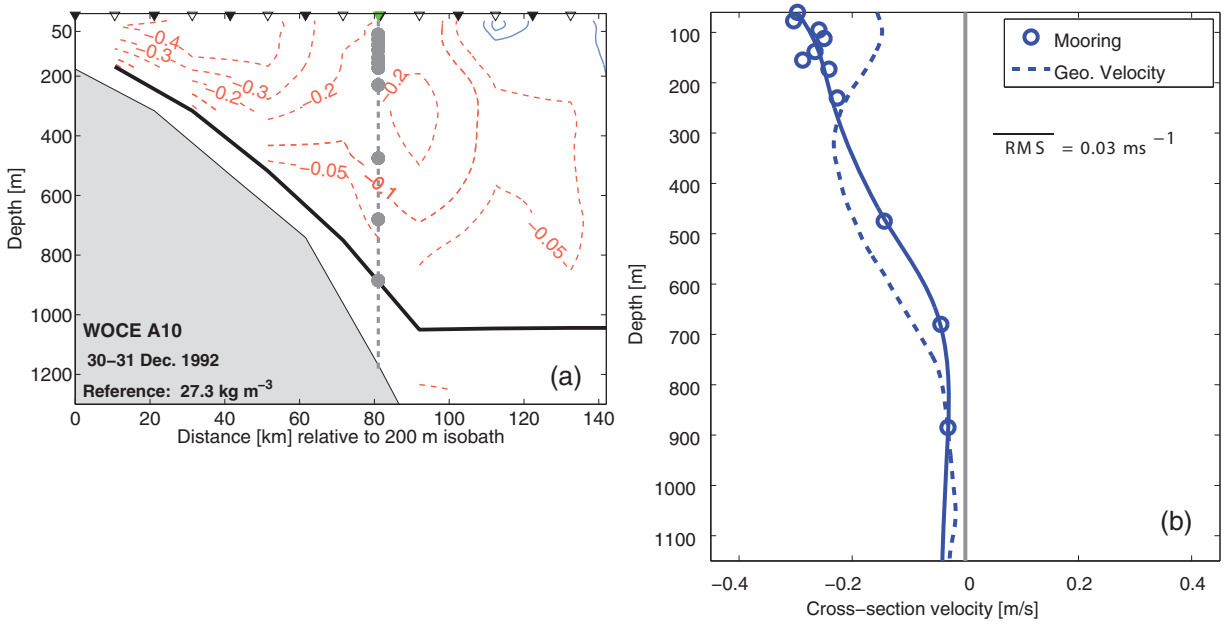

Figure 10. Similar to Figure 7, but for the WOCE A10 cruise and W333 mooring.

mooring, no significant northward flow is observed underneath the BC. At this location, the BC geostrophic transport is estimated as 10.02 Sv. As for the COROAS HM3 cruise, this is likely a lower bound on the BC transport since substantial flow seems to occur over the outer shelf. This estimate is consistent with the lowest transport value presented in the literature; the few estimates of transport in this region range from 11.4 to 27 Sv [*Garfield*, 1990; *da Silveira et al*., 2000], depending on the reference level adopted. The geostrophic velocity is fairly representative of the current meter velocity, with the former slightly underestimating the latter near the surface (Figure 10b). The RMS difference between the two velocity profiles is 0.03 m s^{-1}.

[36] The description of the time-mean along-front flow (section 2.3) and the quasi-synoptic patterns (section 3) suggests that the BC presents a marked downstream changes in its vertical shear. In order to systematically quantify these changes, we now turn to the analysis of the water column average kinetic energy and its partition between barotropic and baroclinic components. We also use the energetics analysis to estimate the importance of the mesoscale activity in the BC.

4. Energetics

4.1. Kinetic Energy Estimate

[37] An estimate of the water column average kinetic energy per unit mass is given by [*Wunsch*, 1997]

$$\mathrm{IKE}\,(\mathrm{t}) = \frac{1}{2H}\int_{-H}^{0}[u^2(t,z)+v^2(t,z)]dz \approx \frac{1}{2H}\int_{-H}^{0}\sum_{i=0}^{4}([\hat{a}_{ui}(t)\phi_i(z)]^2+[\hat{a}_{vi}(t)\phi_i(z)]^2)dz, \quad (1)$$

where ϕ_i is the ith dynamical mode and $[\hat{a}_{ui}, \hat{a}_{vi}]$ its associated amplitude in $[u, v]$. The series of mode amplitudes is estimated by projecting the instantaneous (discrete) velocity profiles onto the dynamical modes in the same fashion as for the mean velocity profiles (section 2.3). Expanding the right-hand side of equation (1), and using the orthonormality condition (for details see *Wunsch* [1997]), we obtain

$$\mathrm{IKE}\,(\mathrm{t}) = \frac{1}{2H}\sum_{i=0}^{4}[\hat{a}_{ui}^2(t)+\hat{a}_{vi}^2(t)]. \quad (2)$$

[38] Equation (2) allows us to estimate the partition of IKE across the dynamical modes. In particular, we are interested in the partition between the barotropic ($\mathrm{IKE}_{bt} = \mathrm{IKE}_0$) and baroclinic ($\mathrm{IKE}_{bc} = \sum_{j=1}^{4}\mathrm{IKE}_j$) components. Similar calculations are performed for the velocity anomalies ($[u', v']$), producing estimates for the water column average eddy kinetic energy (IEKE) and its barotropic/baroclinic partition ($\mathrm{IEKE}_{bt}/\mathrm{IEKE}_{bc}$).

[39] In addition, the surface kinetic energy (SKE) and surface eddy kinetic energy (SEKE) are estimated by plugging $z = 0$ into equation (1). Note that SKE is only separable amongst the dynamical modes if the modes are not correlated in time [*Wunsch*, 1997]. This seems not be the case here. Nonetheless, we keep the total SKE and SEKE in order to compare against those estimates from drifters buoys by *Oliveira et al*. [2009].

Table 7. Time-Mean Water Column Average Kinetic Energy ($\overline{IKE}$) and Eddy Kinetic Energy ($\overline{IEKE}$), and Time-Mean Partition of $\overline{IKE}$ and $\overline{IEKE}$ Between Barotropic and Baroclinic Components

Mooring	$\overline{IKE}$ ($m^2 s^{-2}$)	BT (%)	BC (%)	$\overline{IEKE}$ ($m^2 s^{-2}$)	BT (%)	BC (%)
MARLIM	0.038	30.54	69.46	0.019	41.37	58.63
DFBS	0.037	50.72	49.28	0.022	56.12	43.88
C3	0.045	30.80	69.20	0.014	56.56	43.44
W333	0.032	53.77	46.23	0.014	59.84	40.15

4.2. Kinetic Energy Time Average

[40] First, we explore the time-mean values of IKE and IEKE, and their partition between barotropic and baroclinic components (Table 7). On average, the C3 mooring presents the highest IKE level (0.045 $m^2 s^{-2}$), followed by the MARLIM mooring (0.038 $m^2 s^{-2}$), the DFBS mooring (0.037 $m^2 s^{-2}$), and the W333 mooring (0.032 $m^2 s^{-2}$). However, as stated in section 2.2, this may be influenced by the relative distance of the moorings from the BC core; caution should be taken when comparing these results in absolute values.

[41] An interesting result is the magnitude of the IEKE and its ratio to the IKE. On average, at the MARLIM mooring, the IEKE is estimated as 0.019 $m^2 s^{-2}$, half the magnitude of the IKE. High levels of IEKE are observed at the DFBS mooring (0.022 $m^2 s^{-2}$), and its ratio to the IKE is ~0.6. The C3 mooring presents a relatively weaker (but substantial) IEKE (0.014 $m^2 s^{-2}$; its ratio to the IKE is ~0.33. Farther south, at the W333 mooring, a similar level of IEKE is found (0.014 $m^2 s^{-2}$), though its ratio to the IKE is 0.44. Although these IEKE levels are generally less than those observed in the Gulf Stream and the Kuroshio regions [e.g., *Wunsch*, 1997], their relative importance to the IKE is a remarkable feature of the BC off southeast Brazil. Thus, these results highlight (and in fact quantify) the importance of the mesoscale eddy field in the BC path off southeast Brazil, consistent with the previous studies based on quasi-synoptic observations [e.g., *Campos et al*., 1995], mooring data [*da Silveira et al*., 2008], surface drifters [*Oliveira et al*., 2009] and SST imagery analysis [*Lorenzzetti et al*., 2009]. In particular, these estimates suggest the dominance of the eddy field at the DFBS mooring.

[42] The SKE estimates are 0.113, 0.150, 0.163, and 0.100 $m^2 s^{-2}$ at the DFBS, MARLIM, C3, and W333, respectively. The SEKE/SKE ratios are 0.98, 0.64, 0.20, and 0.40 at the four moorings. Interestingly, at the DFBS and, to some extent, at the MARLIM mooring, the eddy kinetic energy represents a greater fraction of the total kinetic energy at the surface, consistent with the fact that the anomalies are very surface intensified at these locations [*da Silveira et al*., 2008, this study].

[43] It is difficult to compare absolute values of these estimates against those of *Oliveira et al*. [2009]; while we estimate the SKE and SEKE in a single position, those authors have taken averages of drifter-derived velocity over 0.5° × 0.5° bins. Nonetheless, our results are in general agreement with those of the cited authors, specifically in presenting high levels of SEKE at ~22°S–23°S (their

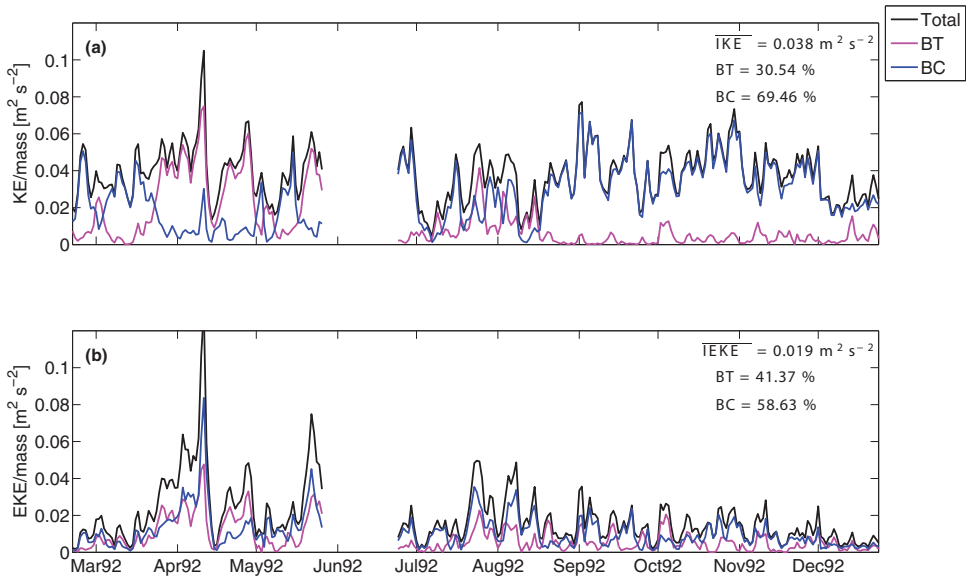

Figure 11. Time series of water column average kinetic energy at the MARLIM mooring (22.7°S). (a) Total kinetic energy (KE). (b) Eddy kinetic energy (EKE). The fractions of energy (KE and EKE) in barotropic (bt) and baroclinic (bc) components are presented in magenta and blue, respectively. $\overline{IKE}$ ($\overline{IEKE}$) represents the average over time of IKE (IEKE). The temporal average of the percentage of IKE and IEKE in barotropic and baroclinic components is also shown.

transects IV and V, close to the DFBS and MARLIM moorings, respectively) and relatively lower SEKE levels at ∼25°S and ∼28°S (their transects VI and VII, close to the C3 and W333 moorings, respectively).

4.3. Barotropic/Baroclinic Partition

[44] At the MARLIM mooring, on average, the IKE is 70% baroclinic (mainly first mode); the IEKE is slightly more barotropic (40%) than IKE. Based on synoptic direct velocity measurements, *da Silveira et al*. [2004] estimate that the BC is 75–80% baroclinic, while *da Silveira et al*. [2008], using 152 days of the MARLIM series, indicate that the along-front BC is 98% baroclinic. We emphasize that our barotropic/baroclinic estimates are based on the IKE; as the cross-front component is mainly due to the eddy field, which is more barotropic, the partition will be more barotropic than the estimates based only on the along-isobath velocity component. Also, we appended the first 150 days of the MARLIM record, which is marked by strong mesoscale activity, and likely contributes to these discrepancies. At the DFBS mooring, on average, a virtual equipartition between barotropic and baroclinic energy for the total flow is observed, likely owing to the dominance of the eddy field. Indeed, the kinetic energy partition is almost the same (∼56% barotropic) for the velocity anomaly field.

[45] At the C3 mooring, on average, the total flow presents a partition similar to that for the MARLIM mooring (∼69% baroclinic). However, its eddy field seems much more barotropic (∼56%). In contrast, at the W333, a dramatic change in the IKE partition is observed; the total flow becomes ∼54% barotropic, confirming our qualitative estimate based on the mean along-front velocity profiles (section 2.3). In this case, on average, the eddy field is just slightly more barotropic (∼59%). While the relatively high barotropicity of the total flow at the DFBS mooring is likely due to the dominance of the eddy field over the mean flow [*Oliveira et al*., 2009, this study], this phenomenon seems to be a manifestation of the high barotropicity of the mean flow itself at the W333 mooring (Figure 6).

4.4. Duration of Eddy Events

[46] The results presented in sections 4.2 and 4.3 represent statistical estimates. However, the kinetic energy level in a given day departs significantly from the time mean. At the MARLIM mooring, strong eddy events that occur at the beginning of the series (April to May 1992) do not repeat in the end (Figure 11). These events are associated with reversals in the surface velocity vector in the BC domain (Figure 1). At the DFBS, C3, and W333 moorings (Figures 12–14), strong energetic events seem to occur throughout the series; in that sense, the series are statistically more homogeneous at these moorings. Typically, bursts of energy in the barotropic mode are associated with energetic eddy events at all moorings.

[47] At the MARLIM mooring, one such event lasts for ∼37 days (March to April 1992). Two similar long-lived barotropic energy events are observed at the DFBS mooring, lasting ∼28 days (April to May 2003) and ∼32 days (August to September 2003). Indeed, these events are marked by strong surface current vector reversals (Figures 11 and 12). In particular, the event depicted at the MARLIM mooring contrasts with the latter 120 days of the record, when the total flow is essentially baroclinic and low levels of IEKE are observed. Thus, there seems to be two regimes at the MARLIM mooring: (1) a "mean regime" (*not* perturbed), characterized by relatively low IEKE levels, and mainly baroclinic total flow; and (2) a "meandering regime" (perturbed), marked by high IEKE levels, and therefore strongly barotropic total flow. In (1), the BC is well defined and prone to baroclinic instability [*da Silveira*

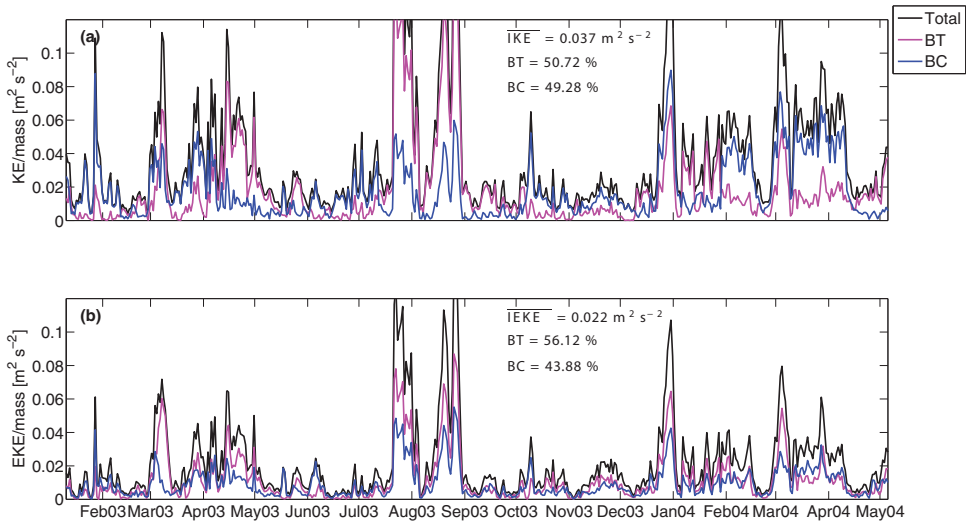

Figure 12. Similar to Figure 11, but at the DFBS mooring (24.15°S).

et al., 2008; *Mano et al*., 2009]; (2) may be linked to the cyclonic meander growth process [*da Silveira et al*., 2008; *Mano et al*., 2009]. The transition from (2) to (1) may be related to the BC (re)stabilization [*Mano et al*., 2009].

[48] Although a similar "meandering regime" is observed at the DFBS mooring, a "mean regime" is not clearly depicted at this location. Relatively quiescent periods are likely solely to be time windows between periods of strong meandering activity. *Oliveira et al*. [2009] failed to depict a statistically significant mean alongshore current at this location. This fact is also consistent with the BC thermal front analysis by *Lorenzzetti et al*. [2009, Figures 1–3], who showed that the BC front presents a spread-out frontal density just past Cape Frio, thus reflecting the high variability of the BC at that location.

[49] At the C3 and W333 moorings, these events are relatively short lived, lasting less than 20 days at maximum. These energetic eddy events may be related to meander propagation between ∼24°S and ∼28°S as suggested by PE numerical simulations [*Campos et al*., 2000; *Fernandes et al*., 2009].

5. Linear Stability Analysis

[50] In order to investigate possible dynamical implications of the downstream changes in the BC, we employ a one-dimensional QG model to study the stability of the mean flow to small perturbations on an along-front *f*-plane channel. The model is similar to that used by *da Silveira et al*. [2008], who built on *Johns* [1988]. Tests were made with a more generalized model, which uses both meridional and zonal velocity components on a β-plane. The instabilities in this generalized model presented maximum growth rates approximately along the mean BC thermal front direction, and the linear instability properties were very close to those obtained with the one-dimensional channel model. Therefore, we maintain the use of the one-dimensional version on a *f*-plane for the sake of simplicity.

5.1. Model Formulation and Simplification

[51] The formulation of the model is standard. We linearize the QG potential vorticity equation about the local mean stratification and velocity profiles [e.g., *Vallis*, 2006]

$$\left[\frac{\partial}{\partial t}+V\frac{\partial}{\partial y}\right]q'-\frac{\partial\psi}{\partial y}\frac{\partial Q}{\partial x}=0,\quad -H<z<0, \tag{3}$$

where

$$\frac{\partial Q}{\partial x}=\frac{\partial}{\partial z}\left(\frac{f_0^2}{N^2}\frac{\partial V}{\partial z}\right), \tag{4}$$

is the mean cross-front QG potential vorticity gradient, and

$$q'=\nabla^2\psi+\frac{\partial}{\partial z}\left(\frac{f_0^2}{N^2}\frac{\partial\psi}{\partial z}\right), \tag{5}$$

is the eddy QG potential vorticity. V is the mean along-front velocity and ψ is the eddy stream function. We have neglected the relative vorticity of the mean flow under the local approximation. This is a valid assumption provided the stretching term is much larger than the relative vorticity of the mean flow. Considering a theoretical jet, *Johns* [1988] showed that the mean relative vorticity in the Gulf Stream off Cape Hatteras was not able to reverse the mean potential vorticity gradient based only on the stretching term. *Johns* [1988] argued that the inclusion of the relative vorticity of the mean flow would not introduce qualitatively differences in the stability properties. Barotropic and mixed instabilities are likely important in the BC [*Oliveira et al*., 2009], but are not considered here owing to the limitation of our data set (one mooring at each location).

[52] Neglecting surface friction and other atmospheric fluxes, the buoyancy anomaly is an invariant at the upper boundary [*Vallis*, 2006]

$$\left[\frac{\partial}{\partial t}+V\frac{\partial}{\partial y}\right]\frac{\partial\psi}{\partial z}-\frac{\partial\psi}{\partial y}\frac{\partial V}{\partial z}=0 \text{ at } z=0, \tag{6}$$

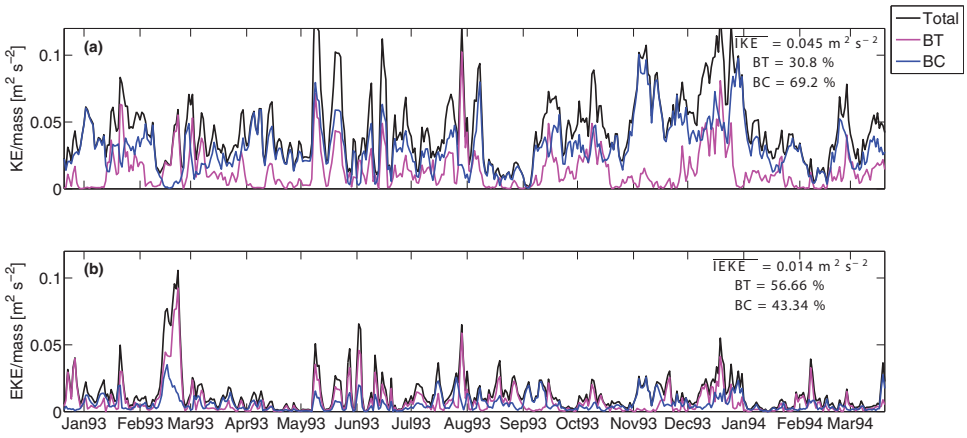

Figure 13. Similar to Figure 11, but at the C3 mooring (25.5°S).

and, ignoring bottom friction, the buoyancy anomaly is forced solely by the flow against topographic gradients at the lower boundary [*Vallis*, 2006]

$$\left[\frac{\partial}{\partial t}+V\frac{\partial}{\partial y}\right]\frac{\partial\psi}{\partial z}-\frac{\partial\psi}{\partial y}\left[\frac{\partial V}{\partial z}+\frac{N^2}{f_0}\frac{\partial\eta_b}{\partial x}\right]=0 \text{ at } z=-H, \quad (7)$$

where $\partial\eta_b/\partial x$ is the cross-front topographic gradient, which was estimated from ETOPO2. For consistency with the QG scaling, we scale the topographic gradients by the Rossby number (Ro) [*da Silveira et al*., 2008]. Based on *da Silveira et al*.'s [2008] estimates, we assume $\mathrm{Ro}=10^{-1}$ for all moorings.

[53] The perturbations are confined in a channel of width $2L$. No-normal flow is imposed at the lateral boundaries

$$\frac{\partial\psi}{\partial y}=0 \text{ at } x=\pm L. \quad (8)$$

[54] Note that in the real ocean no such lateral boundaries exist, and this arbitrarily imposes a cross-front maximum scale for the perturbations [*Johns*, 1988].

[55] Assuming wave-like solutions for the eddy stream function [e.g., *Pedlosky*, 1987; *Vallis*, 2006] leads to a generalized eigenproblem for the complex frequency $(\omega=\omega_r+i\omega_i)$ and eddy stream function vertical structure $[\varphi(z)]$. The instabilities grow exponentially when their frequency has positive complex part (i.e., $\omega_i>0$). For the unstable modes, the vertical structure $[\varphi(z)]$ is complex valued and can be written as

$$\varphi(z)=|\varphi(z)|e^{i\theta(z)}, \quad (9)$$

where $|\varphi(z)|$ is its amplitude and $\theta(z)$ its phase. Under a finite-amplitude assumption $e^{\omega_i t}$, ought to equilibrate at some time [*Pedlosky*, 1987]. In the real ocean, these instabilities are either damped by friction or experience nonlinear cascades [*Vallis*, 2006]. The full development of the instabilities is completely nonlinear [*Pedlosky*, 1987]. Therefore, the predictions presented here should be considered as rough approximations for the initial stages of the instability phenomena in the BC. We chose to use the linear QG approach because it proved to produce consistent predictions for time and length scales of the mesoscale variability in the global ocean [e.g., *Tulloch et al*., 2011], in the

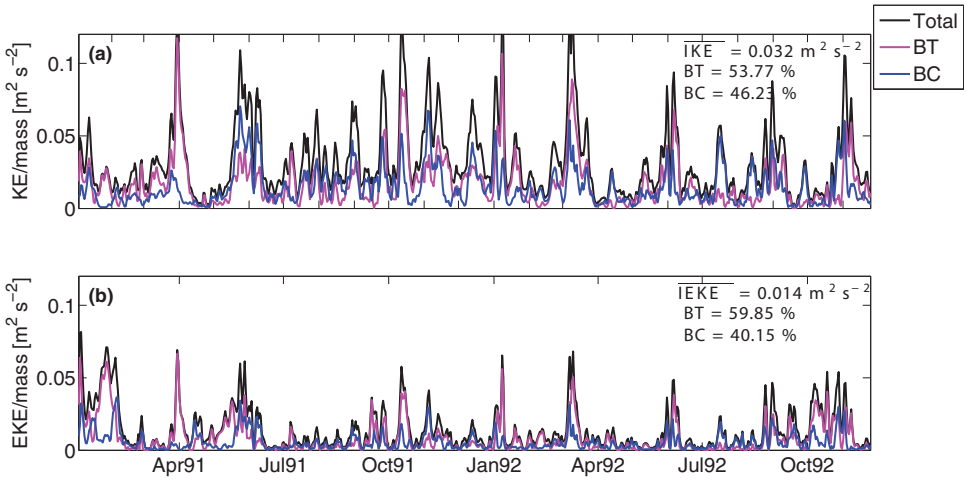

Figure 14. Similar to Figure 11, but at the W333 mooring (27.9°S).

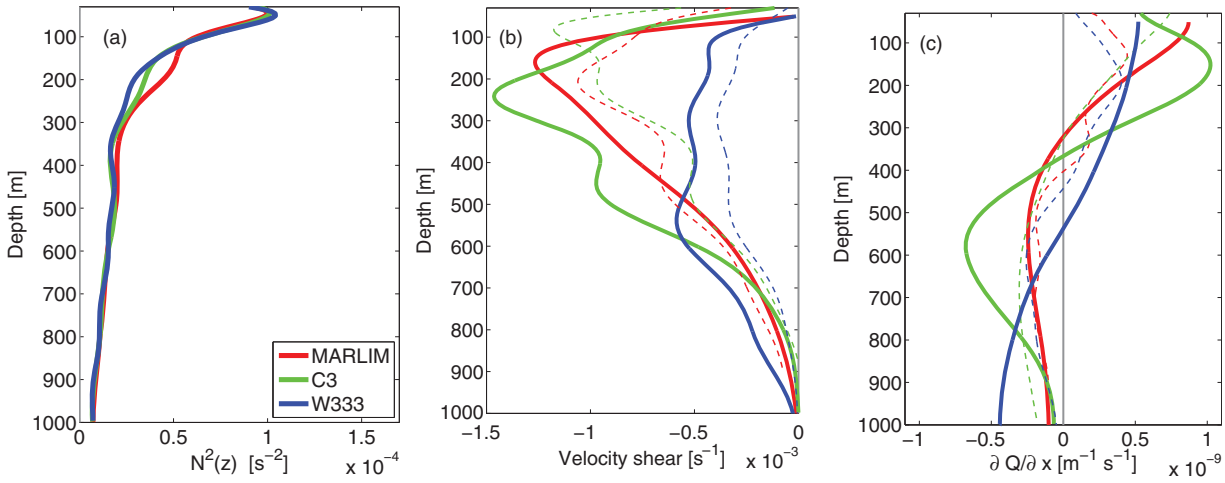

Figure 15. (a) Climatological stratification, (b) mean along-isobath velocity vertical shear, and (c) cross-stream mean potential vorticity gradient for the MARLIM, C3, and W333 moorings. Continuous curves represent those quantities estimated from the mean mooring velocities. Dashed lines stand for profiles estimated from the hydrographic quasi-synoptic fields (averaged over the whole current).

Gulf Stream off Cape Hatteras [*Johns*, 1988] and in the BC System within the Campos Basin [*da Silveira et al*., 2008].

[56] For each mooring, the eigenproblem is solved numerically for a range of wavelengths spanning 10–1000 km. Similarly to *da Silveira et al*. [2008], we use the mean along-front velocity profile synthesized using the dynamical modes (section 2.3; Figure 6). As the mean along front at the DFBS mooring presents low statistical significance, the stability analysis at this location would be very inaccurate. Therefore, we perform the stability analysis only for the MARLIM, C3, and W333 moorings. The mean stratification is taken as the climatological profile (Figure 15a).

[57] We set $L = 100$ km which represents the average width of the BC [*da Silveira et al*., 2008]. Tests for different *L*s were performed. The results proved insensitive to values greater than 100 km in agreement with *Johns* [1988].

5.2. Necessary Conditions for Baroclinic Instability

[58] Before we show the results for the linear stability analysis, it is interesting to evaluate whether the necessary (but not sufficient) conditions for baroclinic instability are satisfied. Generically, one can say that if the mean potential vorticity gradient ($\partial Q/\partial x$) changes its sign within the (vertical) domain, all necessary conditions for baroclinic instability are fulfilled [e.g., *Johns*, 1988]. At the three moorings, $\partial Q/\partial x$ reverts the sign within the water column (Figure 15c). Therefore, the BC is potentially baroclinically unstable at those locations. The $\partial Q/\partial x$ profile is different in magnitude and depth of zero crossing at each mooring. Thus, differences in the baroclinic unstable modes are expected. The $\partial Q/\partial x$ zero-crossing depth occurs at 321, 366, and 538 m at the MARLIM, C3, and W333 moorings, respectively.

[59] In fact, the differences in the $\partial Q/\partial x$ profiles are linked to differences in the velocity shear ($\partial V/\partial z$) profile (Figure 15b), which is a consequence of the downstream thickening of the BC. The $\partial V/\partial z$ is intensified near the surface at the MARLIM and C3 mooring, and middepth intensified at the W333 mooring. The $\partial V/\partial z$ magnitude is greater at the MARLIM and C3 moorings than at the W333 mooring. The maximum $\partial V/\partial z$ magnitude is observed at the C3 mooring (slightly greater than that of the MARLIM mooring).

[60] An important question is whether these local mooring profiles represent $\partial Q/\partial x$ over the whole current. In order to evaluate that we compare these profiles with those estimated from the cross-stream averaged quasi-synoptic hydrographic field. As the quasi-synoptic data are noisy, we use the climatological $N^2(z)$ profile at each region, and project the mean geostrophic velocity profile onto the dynamical modes before computing $\partial V/\partial z$ and $\partial Q/\partial x$. At all locations, the mean geostrophic velocity shear is consistent with that from the moorings. The zero crossing in the $\partial Q/\partial x$ profile is slightly shallower in the quasi-synoptic estimates for C3 and W333, and deeper for MARLIM. Nonetheless, the quasi-synoptic profiles are fairly consistent with those derived from the mean mooring velocity. Therefore, the overall results of the local linear stability analysis are deemed semiquantitatively representative of the whole current.

5.3. Linear Instability Properties and Baroclinic Conversion

[61] The BC is indeed unstable at mesoscales at all moorings (Figure 16). (Only modes with growth rate bigger than 0.005 day^{-1} are considered unstable.) At the MARLIM mooring, the most unstable mode (230 km) has a growth rate of 0.035 day^{-1}, corresponding to an e-folding growth time scale (eT) of about 29 days. At the C3 mooring, the BC is unstable for waves from 100 to 560 km, with a maximum growth rate of 0.056 day^{-1} (corresponding to an eT of 20 days) at 190 km. Farther downstream, at the W333 mooring, the BC is unstable to QG waves from 100 to 400 km. At this mooring, the most unstable mode (180 km) has a growth rate of 0.030 day^{-1}, or an eT of 33 days.

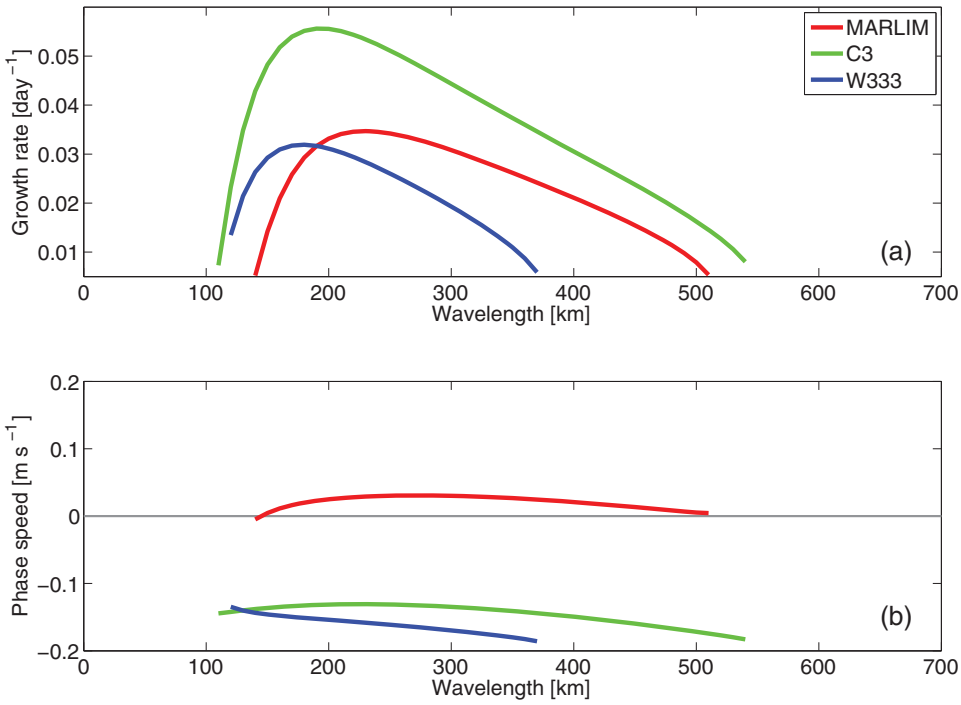

Figure 16. Linear baroclinic instability properties for MARLIM, C3, and W333 moorings: (a) growth rate and (b) phase speed.

[62] The unstable modes at the MARLIM mooring (Figure 16b) have very small phase speeds—e.g., 0.03 m s $^{-1}$ for the most unstable mode (230 km)—similar to those obtained by *da Silveira et al*. [2008]. Conversely, the unstable modes present significant phase speeds at the C3 and W333 moorings, in which the most unstable modes propagate phase with −0.13 and 0.15 m s $^{-1}$, respectively. The steering level (depth at which $Cr = V(z)$ [*Vallis*, 2006]) for the most unstable modes are 365, 380, and 486 m for the MARLIM, C3, and W333 moorings, respectively. The steering level is slightly deeper (shallower) than the depth at which $\partial Q/\partial x$ changes sign at the MARLIM/C3 (W333) moorings. Hence, it is located at the negative (positive) region of $\partial Q/\partial x$ at the MARLIM/C3 (W333) moorings. Based on necessary conditions for baroclinic instability, *Johns* [1988] stated that having the steering at a depth at which the PV gradient is negative seems to be a necessary (but not sufficient) condition for a given mode to be unstable in the Gulf Stream near Cape Hatteras. *Johns* [1988] argued that the reason for such a "requirement" is that the PV gradient is largely positive near the surface. Indeed, this is consistent with the conditions at the MARLIM and C3 moorings, where (absolute) values of $\partial Q/\partial x$ at depth are almost half of its near-surface values. Conversely, at the W333 mooring, $\partial Q/\partial x$ is almost symmetric about its zero crossing. Hence, the unstable modes at this location can have steering levels either shallower or deeper than the $\partial Q/\partial x$ zero crossing.

[63] The vertical structures for the fastest growing mode at each of the three moorings are displayed in Figure 17. The amplitudes of these modes at the MARLIM and C3 moorings are surface intensified and exhibit a sharp decay within the upper 250 and 350 m, respectively. On the other hand, at the W333 mooring, the most unstable mode vertical structure magnitude decreases from surface to middepth (500 m) and then increases toward deeper levels, characteristic of middepth "Phillips-like" instabilities (according to the *Tulloch et al*. [2011] terminology), in which solely $\partial Q/\partial x$ plays a role in its development. The maximum phase shift is shallower at the MARLIM mooring than at the W333 mooring (Figure 17b). An intermediate maximum phase shift is observed at the C3 mooring. Indeed, this phase tilt against the shear of the mean flow is necessary for the conversion of the available potential energy of the mean flow into eddy kinetic energy [e.g., *Vallis*, 2006]. It is interesting to evaluate the rate of baroclinic conversion at each location. An estimate for such a conversion [for details see *Smith*, 2007] is given by

$$G = \int_{-H}^{0} R(z)dz, \tag{10}$$

with

$$R(z) = \frac{V_e^2 \rho_0}{2} \frac{f_0^2}{N^2} \frac{d\theta}{dz} \left(\frac{|\varphi|}{|\varphi|_{max}} \right)^2 \frac{1}{l} \frac{dV}{dz}, \tag{11}$$

where l is the along-front wavenumber, $\rho_0 = 1025$ kg m^{-3} is the reference density, and V_e is the maximum eddy velocity. We assume $V_e = 0.1$ m s^{-1} at all locations. This value is of the order of magnitude as the RMS of the surface velocity anomalies at all moorings (Tables 2, 4, and 5).

[64] At all moorings, the energy conversion for the most unstable mode is positive (mean-to-eddy) throughout the

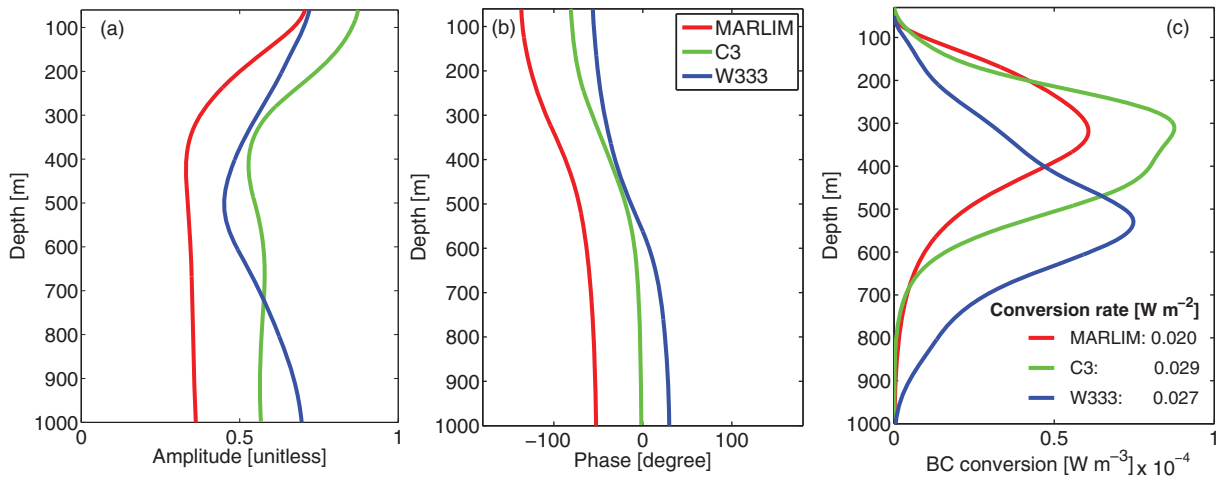

Figure 17. (a) Amplitude ($|\varphi|$), (b) phase (θ), and (c) baroclinic conversion for the most unstable mode at the MARLIM, C3, and W333 moorings. Note that the curves in Figure 17c represent the energy conversion (W m $^{-3}$) as a function of depth [$R(z)$]; the conversion rate [G (W m $^{-2}$); the integral of $R(z)$] also shown.

whole water column (Figure 17c). This result is to be expected since the shear of the mean flow is negative across the whole water column, and the phase of the fastest growing mode tilts monotonically with depth. The maximum conversion depth is much greater (530 m) at the W333 mooring than at the MARLIM (319 m) and C3 (310 m) moorings. Also, this depth of maximum baroclinic conversion is shallower (deeper) than the steering level at the MARLIM/C3 (W333) moorings.

[65] The integral conversion rates (G) at the three moorings (0.020–0.029 W m^{-2}) is comparable in magnitude to those estimates for the Gulf Stream, Kuroshio, and Antarctic Circumpolar Current (0.01–0.05 W m^{-2}) [*Smith*, 2007]. Indeed, the southeast Brazil seems to present high number of eddies [*Chelton et al*., 2007, Figure 3a]. Finally, G is greater at the C3 and W333 moorings (0.029 and 0.027 W m^{-2}, respectively) than at the MARLIM mooring (0.020 W m^{-2}), suggesting that the most unstable modes are slightly more efficient in extracting energy from the mean flow at those locations.

5.4. Comparison Against Observations

[66] An important question is how the results from the linear stability analysis relate to the observed downstream changes of the BC mesoscale fluctuations. No observational information on meander growth and propagation in the BC exists to date as is available for the Gulf Stream [*Johns*, 1988]. Hence, such comparison in the BC System is qualitatively and limited to the vertical structure. We compare the vertical structure of the theoretical predictions against that of the observations. For the former, we have $Va(z) \sim \mathcal{R}e\{|\phi(z)|e^{i\theta(z)}\}$, where Va is the vertical structure of the velocity field due to the most unstable mode. The latter is taken as the spatial structure of the first EOF of the velocity anomalies synthesized using the dynamical modes. The first EOF accounts for 82–92% of the total variance at all locations.

[67] The vertical structure of the fastest growing modes at the MARLIM and C3 moorings decay exponentially from the surface, consistent with the first EOF (Figure 18). At the W333 mooring, the first EOF presents a gentler vertical decay, roughly consistent with the most unstable mode at this location (Figure 18).

[68] We also evaluate how the most unstable modes project onto the dynamical modes. Accordingly, the fastest growing mode is slightly more barotropic at the W333 mooring (67%) than at the MARLIM and C3 moorings (58% and 52%, respectively), only qualitatively consistent with the statistics for the *IEKE* (Table 7). Hence, in general, the linear stability model is deemed successful in predicting qualitative downstream changes in the BC mesoscale fluctuations.

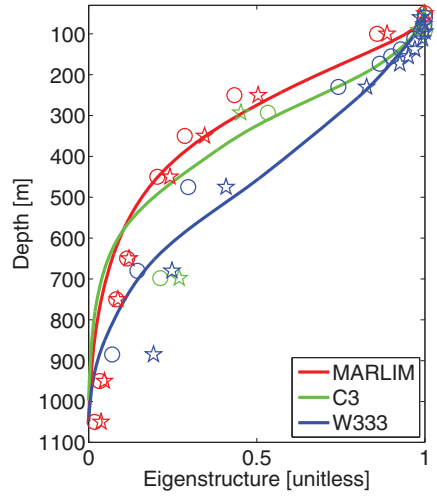

Figure 18. Comparison of the vertical structure of the most unstable modes from the linear stability analysis (continuous lines) against the first EOF from the synthesized velocity anomalies. Circles (stars) represent the first EOF of the cross-front (along-front) velocity anomalies.

6. Summary and Discussion

[69] The goal of the present work is to investigate the downstream changes in the BC as it flows off southeast Brazil (22°S–28°S). We analyze four current meter mooring records spanning this region, namely the MARLIM (22.7°S), DFBS (24.15°S), C3 (25.5°S), and W333 (27.9°S). The mooring data depict the downstream growth in vertical extension of BC. The 350 m deep flow at the MARLIM mooring becomes an 850 m deep flow at the W333 mooring; an intermediate scenario is observed at the C3 mooring, namely a 550 m deep BC. At the DFBS mooring, the mean BC extends down to 400 m, although the mean estimate at this location has low statistical significance owing to the high variability. At the MARLIM mooring, the BC is also highly variable, presenting a standard deviation that exceeds the mean at the uppermost instrument. Conversely, northeastward flowing IWBC proved much less variable at the MARLIM mooring. Farther downstream, the entire water column over the slope seems to flow to the southeast. Therefore, the Santos bifurcation seems to occur somewhere between 25.5°S and 27.9°S, consistent with a recent description on the basis of float trajectories [*Legeais et al*., 2013].

[70] Quasi-synoptic observations contemporary with the mooring records are generally consistent with the scenario that emerges from the mean moored velocity analysis. Geostrophic estimates reveal that the BC transport presents a major increase from the C3 mooring (5.73 Sv) to the W333 mooring (10.02 Sv). Part of this increment is certainly associated with the Santos bifurcation. The presence of a recirculation feeding the BC at about 27°–28°S is not ruled out [*Peterson and Stramma*, 1991; *Stramma and England*, 1999], and may account for a fraction of this transport growth. Furthermore, variabilities of the BC transport on many time scales between the two hydrographic section occupations (∼7 months) can contribute to these differences.

[71] The water column average kinetic energy (IKE) and its barotropic/baroclinic partition estimates reveal that the changes in the BC System vertical structure are accompanied by strong changes in the vertical partition of the IKE. Accordingly, the BC is, on average, highly baroclinic (∼70%) at the MARLIM mooring, in agreement with previous estimates [*da Silveira et al*., 2004] that point the high baroclinicity of the BC System close to this latitude; similar results are obtained at the C3 mooring. A significant change in the partition of the energy is observed to the south of the C3 mooring. The total flow becomes 54% barotropic at the W333 mooring.

[72] The water column average eddy kinetic energy (IEKE) and its ratio to the IKE confirms the importance of the BC mesoscale activity as it flows off the southeast: the IEKE accounts for from 33% (W333 mooring) to 60% (DFBS mooring) of the IKE. This fact is indeed in agreement with quasi-synoptic observations [e.g., *Campos et al*., 1995, 2000; *da Silveira et al*., 2004], drifter statistics [*Oliveira et al*., 2009] and thermal front analysis [*Lorenzzetti et al*., 2009]. Moreover, our analysis suggests that the eddy field dominates the mean flow at the DFBS mooring. The IEKE is, on average, more barotropic than the IKE. The exception is the W333 mooring, where the IEKE has approximate the same energy partition as the total flow (∼59% barotropic).

[73] Indeed, the analysis of the IKE and IEKE time series reveals that these eddy events are associated with bursts of energy in the barotropic mode, thus supporting the idea that the BC meanders are more barotropic than the mean flow [*da Silveira et al*., 2008]. At the MARLIM mooring, the persistence of the energy in the barotropic mode for ∼37 days may be an indication of a quasi-standing meander growth in the region [*da Silveira et al*., 2008; *Mano et al*., 2009]. Similar long-lived eddy events are observed at the DFBS mooring. Conversely, at the C3 mooring, these bursts of energy in the barotropic mode last 20 days at maximum (typically much less), likely owing to meander propagation [*Campos et al*., 2000; *Fernandes et al*., 2009].

[74] We also evaluate the stability of the mean along-front BC to small-amplitude perturbations at the moorings. As far as the baroclinic instability is concerned, the BC downstream vertical extension growth has two major effects on the linear instability properties. First, the unstable waves are slightly but noticeably shorter (∼20%) to the south. The estimated fastest growing modes were associated with wavelengths of 230, 190, and 180 km, at the MARLIM, C3, and W333 moorings, respectively. Second, the unstable waves at the MARLIM mooring present very small phase speeds (∼0.03 m s^{-1}), whereas those at the C3 and W333 moorings have significant propagation speeds (−0.13 and −0.15 m s^{-1}, respectively). These predictions are qualitatively consistent with SST imagery analysis [*Garfield*, 1990] and PE simulations [*Campos et al*., 2000; *Fernandes et al*., 2009]. The theoretical prediction that the vorticity waves are shorter to the south still needs evidence from observations.

[75] The fastest growing modes have vertical structures that resemble the first EOF of the observed velocity anomalies. These modes present rates of baroclinic conversion comparable to those observed in the other strong currents [*Smith*, 2007]. This is consistent with the fact that the IEKE is significant at all moorings. The most unstable modes at the W333 and C3 moorings are more efficient in transferring energy from the mean flow than the fastest growing mode at the MARLIM mooring. This apparently contradicts the fact that the IEKE accounts for a larger fraction of the IKE at the MARLIM mooring (0.5) than at the W333 and C3 moorings (0.44 and 0.3, respectively). However, in interpreting this result, one should bear in mind that this prediction only suggests that a given perturbation would grow more efficiently at the expense of the mean flow at the W333 and C3 moorings. It does not indicate that there are more perturbations at these locations, which may be accounted for by, e.g., local differences in topography and changes in the continental margin orientation [*Campos et al*., 1995].

7. Final Remarks

[76] We conclude by answering the questions posed in section 1: (1a) The BC thickens from a 350 m at 22.7°S to 850 m at 27.9°S; (1b) Hydrographic observations suggest that the BC transport is increased by at least 4.3 Sv from 25.5°S to 27.9°S. (2a and 2b) The total flow is mainly

baroclinic (∼70%) at 22.7°S and 25.5°S, and is mainly barotropic at (∼54%) at 27.9°S; it should be noted that an equipartition is observed for the total flow at 24.15°S, likely a manifestation of the dominance of the eddy field at this location. (3) In a water column average sense, the eddy field accounts for 30–60% of the total kinetic energy. (4a) The changes are twofold: (i) The fastest growing modes are shorter to the south (at 25.5°S and 27.9°S); (ii) at 25.5°S and 27.9°S, these unstable waves tend propagate to the south, as opposed to quasi-standing waves at 22.7°S. (4b) These modes have vertical structures roughly consistent with the observed mesoscale fluctuations.

[77] The most vexing limitation of this paper is that we were not able to quantitatively assess the linear stability predictions owing to lack of information on the BC. Future observational programs should focus on obtaining measurements to estimate of growth rates and propagation speeds of the BC meanders, e.g., by using inverted echo sounder arrays [e.g., *Watts and Johns*, 1982]. One could obtain empirical dispersion relationships; theories could then be quantitatively tested against these estimates.

[78] Finally, barotropic conversions seem to be important along the entire BC path [*Oliveira et al*., 2009]. One important open question concerns the relative importance of the baroclinic and barotropic instability in giving rise to the mesoscale variability of the BC. The full instability process cannot be accounted for by linear models. Therefore, this question should be assessed by combining observations [e.g., *da Silveira et al*., 2008] and primitive-equation (PE) numerical models [e.g., *Mano et al*., 2009]. However, PE models are expected to be consistent with the available statistics for the BC [e.g., *Oliveira et al*., 2009]. We believe that the present estimates could also provide a test bed for those models.

[79] **Acknowledgments.** We acknowledge three anonymous reviewers for their thorough comments that substantially improved this paper. We also thank E.D. Barton (Editor in chief, JGR-Oceans), Amit Tandon (UMassD), José Roberto B. Leite (IOUSP), José Luiz L. de Azevedo (FURG), Marcelo Dottori (IOUSP), Rick Salmon (SIO), Frank "Chico" Smith (UMassD), and Janet Sprintall (SIO) for useful comments, insights, and editorial assistance. The COROAS HM2 data were kindly provided by Edmo Campos (IOUSP). We are also grateful to Petróleo Brasileiro S. A.—PETROBRAS for providing the MARLIM data set and promoting oceanographic research projects. This research was funded by *São Paulo Research Foundation* (FAPESP 2010/13629-6, 2012/02119-2 and 2008/58101-9). ICAS and BMC acknowledge support from CNPq (307122/2010-7).

References

Antonov, J. I., D. Seidov, T. P. Boyer, R. A. Locarnini, A. V. Mishonov, H. E. Garcia, O. K. Baranova, M. M. Zweng, and D. R. Johnson (2010), NOAA Atlas NESDIS 68 WORLD OCEAN ATLAS 2009, vol. 2: Salinity, technical report. march, U.S. Gov. Print. Off., Washington, D. C.

Beckers, J. M., and M. Rixen (2003), EOF calculations and data filling from incomplete oceanographic datasets, *J. Atmos. Oceanic Technol.*, *20*(12), 1839–1856.

Böebel, O., R. E. Davis, M. Ollitraut, R. G. Peterson, P. L. Richard, C. Schmid, and W. Zenk (1999), The intermediate depth circulation of the western South Atlantic, *Geophys. Res. Lett.*, *26*(21), 3329–3332.

Campos, E. J. D., J. E. Goncalves, and Y. Ikeda (1995), Water mass structure and geostrophic circulation in the South Brazil Bight—Summer of 1991, *J. Geophys. Res.*, *100*(C9), 253–250.

Campos, E. J. D., Y. Ikeda, B. M. Castro, S. A. Gaeta, J. A. Lorenzetti, and R. Stevenson (1996), Experiment studies circulation in the Western South Atlantic, *EOS Trans. AGU*, *77*(27), 253–250.

Campos, E. J. D., D. Velhote, and I. C. A. Silveira (2000), Shelf break upwelling driven by Brazil Current cyclonic meanders, *Geophys. Res. Lett.*, *27*(6), 751–754.

Chelton, D. B., M. G. Schlax, R. M. Samelson, and R. A. de Szoeke (2007), Global observations of large oceanic eddies, *Geophys. Res. Lett.*, *34*, L15605, doi:10.1029/2007GL030812.

da Silveira, I. C. A., A. C. K. Schmidt, E. J. D. Campos, S. S. Godoi, and Y. Ikeda (2000), A Corrente do Brasil ao Largo da Costa Leste brasileira, *Rev. Bras. Oceanogr.*, *48*(2), 171–183.

da Silveira, I. C. A., L. Calado, B. M. Castro, M. Cirano, J. A. M. Lima, and A. D. S. Mascarenhas (2004), On the baroclinic structure of the Brazil Current intermediate western boundary current system at 2223S, *Geophys. Res. Lett.*, *31*, L14308, doi:10.1029/2004GL020036.

da Silveira, I. C. A., J. A. M. Lima, A. C. K. Schmidt, W. Ceccopieri, A. Sartori, C. P. F. Franscisco, and R. F. C. Fontes (2008), Is the meander growth in the Brazil Current system off Southeast Brazil due to baroclinic instability?, *Dyn. Atmos. Oceans*, *45*(3–4), 187–207, doi:10.1016/j.dynatmoce.2008.01.002.

Dengler, M., F. A. Schott, C. Eden, P. Brandtl, and R. Zantopp (2004), Break-up of the Atlantic deep western boundary current into eddies at 8°S, *Nature*, *432*, 1018–1020.

Emery, W., and R. Thomson (2001), *Data Analysis Methods in Physical Oceanography*, Elsevier, Amsterdam, the Netherlands.

Evans, D., and S. R. Signorini (1985), Vertical structure of the Brazil Current, *Nature*, *315*, 48–50.

Fernandes, A. M., I. C. da Silveira, L. Calado, E. J. Campos, and A. M. Paiva (2009), A two-layer approximation to the Brazil Current intermediate western boundary current system between 20°S and 28°S, *Ocean Model.*, *29*(2), 154–158, doi:10.1016/j.ocemod.2009.03.008.

Garfield, N. (1990), The Brazil Current at subtropical latitudes, PhD thesis, Univ. of Rhode Island, Kingston.

Glover, D. M., W. J. Jenkins, and S. C. Doney (2011), *Modeling Methods for Marine Science*, Cambridge Univ. Press, Cambridge, U. K.

Johns, W. E. (1988), One-dimensional baroclinically unstable waves on the Gulf Stream potential vorticity gradient near Cape Hatteras, *Dyn. Atmos. Oceans*, *11*, 323–350.

Legeais, J.-F., M. Ollitrault, and M. Arhan (2013), Lagrangian observations in the intermediate western boundary current of the South Atlantic, *Deep Sea Res., Part II*, *85*, 109–126, doi:10.1016/j.dsr2.2012.07.028.

Locarnini, R. A., A. V. Mishonov, J. I. Antonov, T. P. Boyer, H. E. Garcia, O. K. Baranova, M. M. Zweng, and D. R. Johnson (2010), NOAA Atlas NESDIS 68 WORLD OCEAN ATLAS 2009, vol. 1: Temperature, technical report march, U.S. Gov. Print. Off., Washington, D. C.

Lorenzzetti, J. A., J. L. Stech, W. L. M. Filho, and A. T. Assireu (2009), Satellite observation of Brazil Current inshore thermal front in the SW South Atlantic: Space/time variability and sea surface temperatures, *Cont. Shelf Res.*, *29*, 2061–2068.

Mano, M. F., A. M. Paiva, A. R. Torres Jr., and A. L. G. A. Coutinho (2009), Energy flux to a cyclonic eddy off Cabo Frio, Brazil, *J. Phys. Oceanogr.*, *39*, 2999–3010, doi:10.1175/2009JPO4026.1.

Müller, T. J., Y. Ikeda, N. Zangenberg, and L. V. Nonato (1998), Direct measurements of western boundary currents off Brazil between 20°S and 28°S, *J. Geophys. Res.*, *103*(C3), 5429–5437.

Oliveira, L. R., A. R. Piola, M. M. Mata, and I. D. Soares (2009), Brazil Current surface circulation and energetics observed from drifting buoys, *J. Geophys. Res.*, *114*, C10006, doi:10.1029/2008JC004900.

Pedlosky, J. (1987), *Geophysical Fluid Dynamics*, Springer study ed., Springer, New York.

Peterson, R. G., and L. Stramma (1991), Upper-level circulation in the South Atlantic Ocean, *Prog. Oceanogr.*, *26*, 1–73.

Schott, F. A., M. Dengler, R. Zantopp, L. Stramma, J. Fisher, and P. Brandt (2005), The shallow and deep western boundary current circulation of the South Atlantic at 5°S–11°S, *J. Phys. Oceanogr.*, *35*, 2031–2053.

Smith, K. S. (2007), The geography of linear baroclinic instability in Earth's oceans, *J. Mar. Res.*, *65*, 655–683.

Stramma, L., and M. England (1999), On the water masses and mean circulation of the south Atlantic ocean, *J. Geophys. Res.*, *104*(C9), 20,863–20,883.

Stramma, L., J. Fischer, and J. Reppin (1995), The North Brazil Undercurrent, *Deep Sea Res., Part I*, *42*(5), 773–795, doi:10.1016/0967-0637(95)00014-W.

Szuts, Z. B., J. R. Blundell, M. P. Chidichimo, and J. Marotzke (2012), A vertical-mode decomposition to investigate low-frequency internal motion across the Atlantic at 26 N, *Ocean Sci.*, *8*(3), 345–367, doi:10.5194/os-8-345-2012.

Tulloch, R., J. Marshall, C. Hill, and K. S. Smith (2011), Scales, growth rates, and spectral fluxes of baroclinic instability in the ocean, *J. Phys. Oceanogr.*, *41*, 1057–1575.

Vallis, G. K. (2006), *Atmospheric and Oceanic Fluid Dynamics*, 745 pp., Cambridge Univ. Press, Cambridge, U. K.

Watts, D. R., and W. E. Johns (1982), Gulf stream meanders: Observations on propagation and growth, *J. Geophys. Res.*, *87*(C12), 9467–9476, doi: 10.1029/JC087iC12p09467.

Wunsch, C. (1997), The vertical partition of oceanic horizontal kinetic energy, *J. Phys. Oceanogr.*, *27*(1), 1770–1794.